Chemical Engineering Journal 143 (2008) 172–179

Contents lists available at ScienceDirect

Chemical Engineering Journal

journal homepage: www.elsevier.com/locate/cej

Combustion of liquid bio-fuels in an internal circulating fluidized bed

Francesco Miccio[a,*], Sylwester Kalisz[b], David Baxter[b], Karel Svoboda[c]

[a] Istituto di Ricerche sulla Combustione – CNR, Napoli I, Italy
[b] European Commission, Joint Research Centre, Institute for Energy JRC/IE, Petten NL, Netherlands
[c] Institute of Chemical Process Fundamentals, Academy of Sciences, Prague CZ, Czech Republic

ARTICLE INFO

Article history:
Received 9 July 2007
Received in revised form 2 April 2008
Accepted 4 April 2008

Keywords:
Internal circulating fluidized bed
Liquid fuel
Combustion
Gasification
Incineration

ABSTRACT

The paper presents novel experimental results for the combustion of liquid bio-fuels in an internal circulating fluidized bed (ICFB). A 20 kW experimental facility equipped with an air-assisted injector has been used. Reliable operation, high combustion efficiency and limited temperature increase along the combustion riser tube have been attained at different operating conditions. However, CO emission has been rather higher than expected. A form of micro-explosive behaviour of the fuel has been experienced at relatively low bed temperatures (710–730 °C), but this behaviour was significantly less intense than in bubbling fluidized beds. A mathematical model of the combustion of liquid fuels has been adapted to ICFB conditions. The comparison between model and experimental results demonstrates that the efficiency of fuel-air mixing has a crucial role on combustion behaviour. Poor contact between air and fuel in the bottom half of the riser is responsible for high CO levels measured during the experiments.

On the whole, the research demonstrates that the proposed liquid injection process could be suitable for application in co-gasification or for incineration of liquid wastes.

1. Introduction

Combustion of liquid fuels in fluidized beds (FB) has recently been claimed as a way to achieve more homogeneous and controlled temperature distribution as well as to minimise the emissions of some pollutants, like nitrogen oxides and soot [1]. Furthermore, fluidized beds offer the possibility to efficiently burn liquid wastes or raw vegetable oils, even without any preparatory chemical treatment that is normally required for enhancing the atomization behaviour in traditional burners. Encouraging experiences on FB combustion of several liquid fuels have been reported in literature [2–8]. The utilization of an injector, which could be fed with an auxiliary gas or steam stream, is the best option for reliably feeding the fuel into the combustion chamber. In general, the combustor performance can be improved by optimising the choice of operating variables, which include the gas-to-fuel ratio at the injector, as well as by adopting an effective design of the combustion chamber and fuel injection system. In bubbling fluidized beds segregation phenomena [9] can arise as a consequence of the formation of fuel-rich bubbles in the proximity of the injector, leading to massive release of unconverted hydrocarbons above the bed surface and loss of temperature uniformity. Under certain conditions micro-explosions have also been observed during FB combustion of liquid fuels [8,10].

Fluidized beds have been used extensively for air/steam gasification of biomass or waste to produce a valuable syngas containing mainly CO, CH_4, and H_2 and other minor species [11]. Minimizing the nitrogen content is beneficial for the process of the whole cycle of power generation, in particular when fuel cells are used for the conversion of hydrogen rich syngas. So far, the internal circulating fluidized bed (ICFB) concept has been successfully applied for biomass gasification [12,13]. The major advantage of this option is the possibility to carry out the process in two separated but interconnected chambers, where different operating conditions can be set. The two vessels are normally operated under reducing, meaning gasification, and oxidizing, meaning combustion, atmospheres, respectively. Thus, two distinct gas streams are generated: the flue gas exiting the oxidizing/combustion chamber and the syngas exiting the reducing/gasification chamber. The heat transferred from the former to the latter chamber enhances the endothermic fuel conversion in the reducing zone. The main advantage is the production of syngas potentially rich in combustible species and thus with a high heating value, since dilution with nitrogen is avoided. Under certain conditions, when the process requires the supply of external power (e.g. when low-quality fuel is to be gasified or the fuel water content is high), the steady operation can be ensured by co-gasification with an auxiliary fuel (e.g. highly reactive coal). Alternatively, direct injection of a mineral or natural oil into the combustion chamber can be made, this option being

* Corresponding author.
E-mail address: miccio@irc.cnr.it (F. Miccio).

1385-8947/$ – see front matter © 2008 Elsevier B.V. All rights reserved.
doi:10.1016/j.cej.2008.04.002

Nomenclature

A_p	surface/volume ratio of bubble (m^{-1})
c_g	specific heat of gas ($J\,mol^{-1}\,K^{-1}$)
c_s	specific heat of sand ($J\,kg^{-1}\,K^{-1}$)
C	gas concentration ($mol\,m^{-3}$)
d	equivalent orifice size (m)
D_b, D_{sl}	bubble, slug diameter (m)
D_p	particle size (mm)
D_t	riser diameter (m)
e	excess air factor (–)
E	activation energy ($J\,mol^{-1}$)
g	gravity acceleration ($m\,s^{-2}$)
h_{be}	coefficient of thermal exchange in the bed ($W\,m^{-3}\,K^{-1}$)
h_w	coefficient of thermal exchange with the wall ($W\,m^{-2}\,K^{-1}$)
H	bed height (m)
I	input model variable (–)
k	pre-exponential factor ($L^{\nu-1}\,mol^{\nu-1}\,s^{-1}$)
k_t	thermal conductivity ($W\,K^{-1}\,m^{-1}$)
K	constant for bed circulation rate ($kg^{0.5}\,m^{-1}$)
n	number of moles (mol)
O	model output variable (–)
P	pressure (Pa)
Q_0	volumetric flow rate of the fuel/air jet ($m^3\,s^{-1}$)
r	reaction rate ($mol\,m^{-3}\,s^{-1}$)
R	gas-law constant ($J\,mol^{-1}\,K^{-1}$)
t	time (s)
T	temperature (K)
U, U_{mf}	fluidization, minimum fluidization velocities ($m\,s^{-1}$)
U_b, U_{sl}	bubble and slug velocities ($m\,s^{-1}$)
U_t	terminal velocity ($m\,s^{-1}$)
U_0	injection velocity ($m\,s^{-1}$)
V	bubble volume (m^3)
W_{bed}	bed inventory (kg)
W_s	bed circulation rate ($kg\,m^{-2}\,s^{-1}$)
Y_i	molar fraction, (–)
z	elevation (m)

Greek symbols

β_i	stoichiometric coefficient (–)
β_p	coefficient of Ranz and Marshall correlation, ($W\,m^{-2}\,K^{-1}$)
ΔT	temperature increment (K)
ζ	enthalpy of reaction ($J\,mol^{-1}$)
η	combustion efficiency (–)
θ	coalescence time (s)
λ	flame length (m)
ν	reaction order (–)
σ	sensitivity (–)
Φ	bubble frequency in the bed (s^{-1})
Ψ_i	diffusion flux ($mol\,m^{-3}\,s^{-1}$)
Ω_i	molar coalescence rate ($mol\,s^{-1}$)

Subscripts

b	bubble
bed	bed emulsion phase
f	fuel
fr	freeboard
sl	slug bubble phase

easier to implement and resulting in a greater reliability of the process.

The aim of the present research is to study the behaviour of an ICFB combustor/gasifier when it is fired with liquid bio-fuels and to ascertain whether unexpected and undesirable phenomena commonly experienced in bubbling beds are to be expected in ICFBs. The research, having mainly an experimental character, is of interest for both co-gasification of carbonaceous materials and incineration of liquid wastes. A theoretical approach based on a slugging-coalescence mathematical model is also proposed in the paper for understanding and explaining the trends of the experimental results.

2. Experimental

The set-up of the 20 kW experimental facility is shown in Fig. 1. The core of the facility is the internal circulating fluidized bed reactor made of stainless steel AISI-316L. It consists of two coaxial cylindrical vessels with a total height of 2.5 m. The external vessel has two different diameters, 234 mm ID in the lower section and 300 mm ID in the upper section. A flanged conical adapter is fitted between the two columns. A conical gas distributor, having 432 holes with 1.2 mm diameter, is located at the bottom of the external vessel. Several threaded tubes of different sizes are welded perpendicularly to the vessel at almost regular distances along the external vessel to permit gas and fuel feeding, gas sampling, temperature and pressure measurements, and visual access to the interior. The gas exit port is located at a height of 1970 mm above the gas distributor.

The internal vessel (the combustion riser) comprises a 78 mm ID tube, 2185 mm high. Two circular holes (20 mm ID) are located at height 152 mm from the bottom of the riser tube. The holes permit circulation of bed material from the external vessel to the internal vessel. At the bottom of the riser is a changeable gas/fuel injector, sketched in Fig. 2, that is also equipped with three probes for pressure and temperature measurement. The gaseous flow in the inner column enables bed circulation. The separation of entrained particles from the gas stream is accomplished by means of an impactor, high in the riser vessel, after which the bed particles return to the external vessel via a 30 mm orifice located at an elevation of 1380 mm. Both exits from the internal and external vessels are connected to 100 mm ID cyclones, which are respectively connected in sequence to 78 mm filter holders for hot gas de-dusting. Each of the latter are equipped with a ceramic candle filter with a height of 1 m and a mesh size of 1.5 μm. The cyclones and filters are fitted with ball valves at the bottom, to enable the collected particulate matter to be removed. After de-dusting the two gas streams are sent separately to the chimney.

Two feeding lines for compressed air and gas stored in bottles are connected to both reactor vessels for the operation of the two vessels under different atmospheres (e.g. air, O_2 enriched air, N_2, CO_2). Before injection into the internal vessel the gas stream is preheated to 600 °C using an electric heater. Three analogue thermal mass flow instruments are used for measuring and controlling the gas flow rates.

The power for heating up the reactor to the working temperature (700–900 °C), for compensating the heat losses, and for providing the energy in case of allothermal operation is supplied by electrical resistance heaters made from 10 mm OD Incoloy 800 mineral insulated tube. The heaters are installed in direct contact with the external surface of the reactor vessel and provide a maximum power input of 12 kW. An 80 mm thick thermal insulation jacket composed of mineral fibres minimizes the heat losses and ensures protection for workers.

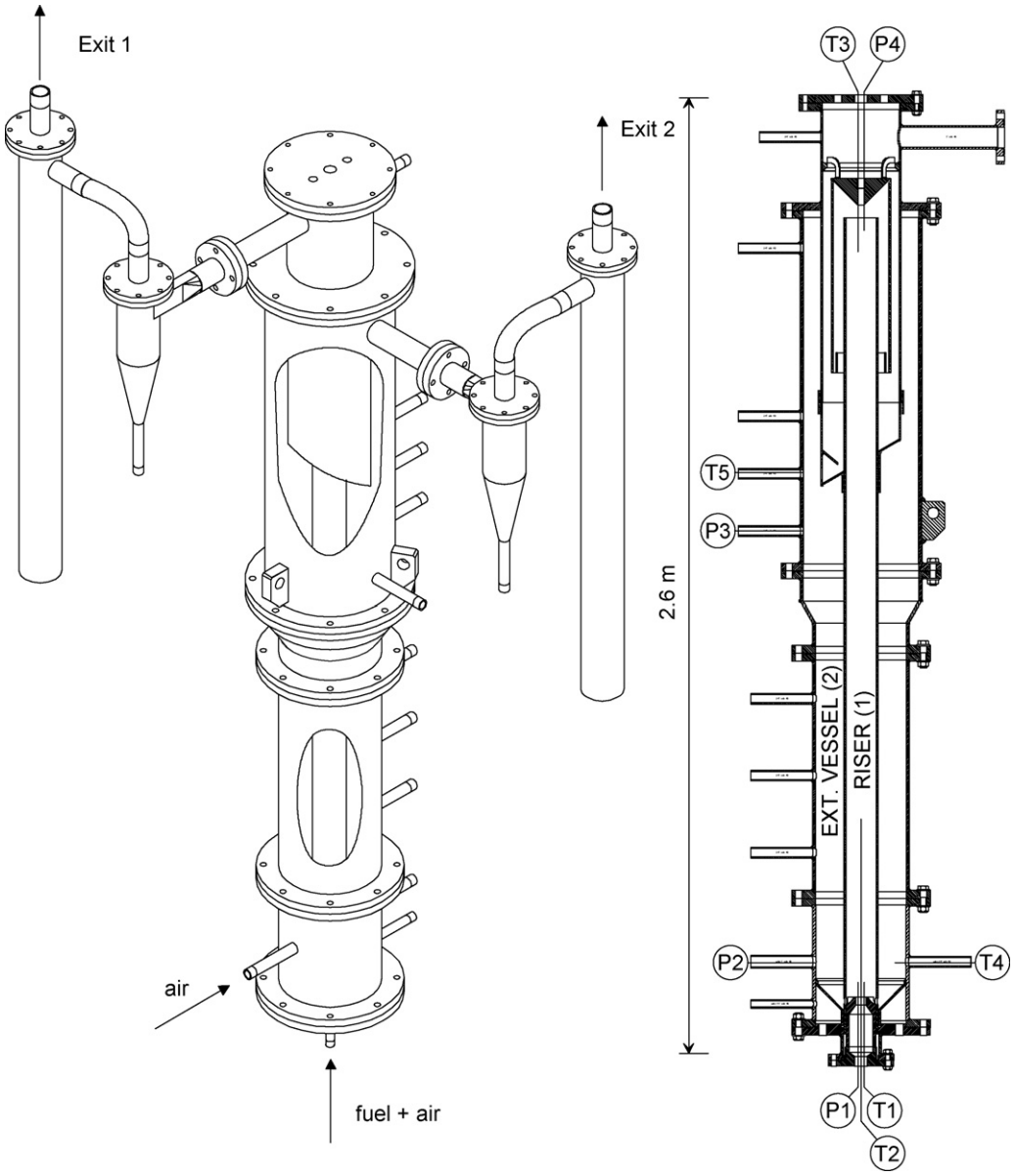

Fig. 1. Experimental rig – internal circulating fluidized bed reactor equipped with a 78 mm ID riser.

Dedicated gas analyzers permit continuous measurement of the concentration of six gas species (O_2, CO_2, CO, H_2, CH_4, NO). The analysers are equipped with an integrated module for pumping, filtering and chilling the gas stream before analysis. The gas stream is alternatively taken from two different points of the facility by means of manually actuated valves, namely at the exit of the internal and external vessels downstream from the ceramic filters.

Sand of quartzite 150–400 μm size range has been used for the experiments having minimum velocity for fluidization equal to 0.025 m/s at 800 °C.

Two bio-fuels, bio-diesel and sunflower oil, have been fired under different operating conditions. They have been directly introduced into the internal vessel by means of a membrane pump with finely adjustable speed and the air-assisted injector shown in Fig. 2; the mass flow rate was determined using an electronic balance. The properties of the fuels are given in Table 1. It is worth noting that the viscosity of the sunflower oil is several times higher than that of the biodiesel.

Table 1
Fuel properties

	Biodiesel	Sunflower oil
Density (40 °C), (kg m^{-3})	868.7	906.4
Kinematic viscosity (40 °C), (mm^2 s^{-1})	4.75	31.70
Higher heating value (MJ kg^{-1})	37.70	39.81
Lower heating value (MJ kg^{-1})	34.86	37.11
Chemical analysis		
C (wt.%)	76.9	77.4
H (wt.%)	11.7	11.2
N (wt.%)	<0.75	<0.75
S (wt.%)	0.06	0.01
O by diff. (wt.%)	10.6	10.6
Ash (wt.%)	<0.01	<0.01
Water content (wt.%)	<0.01	<0.01
Stoichiometric air (Nm^3 kg^{-1})	9.88	9.78

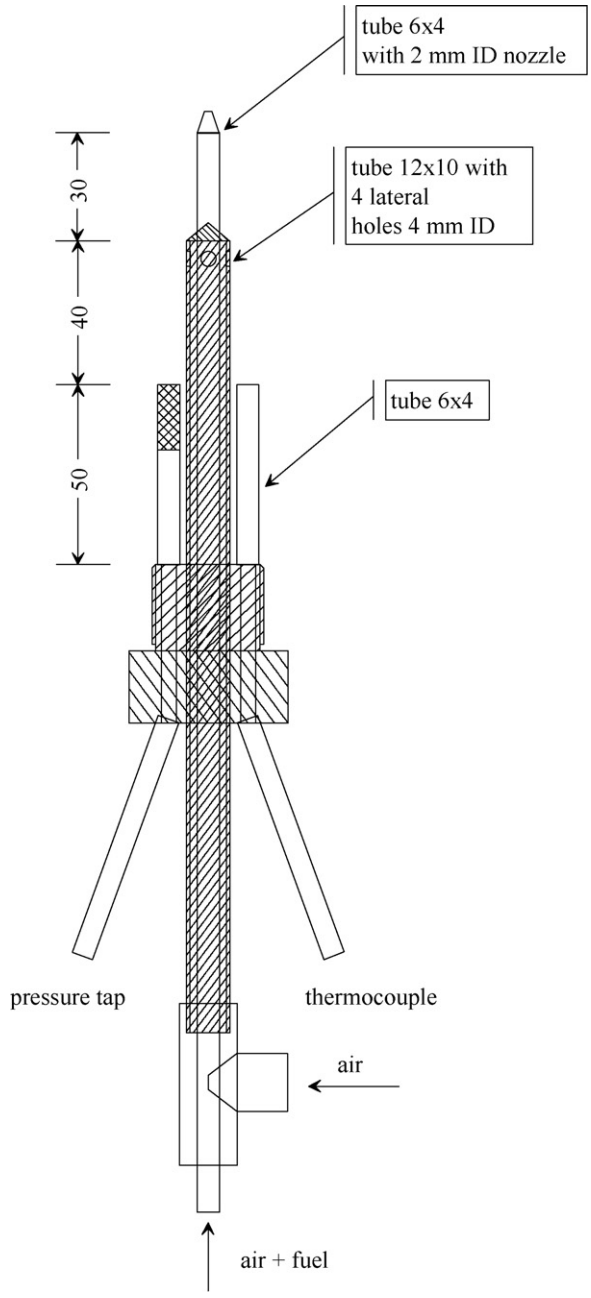

Fig. 2. Air-assisted injector for liquid fuels.

Experiments have been carried out under steady-state conditions. After electric start-up, the fuel was fed as the temperature in the riser exceeded 500 °C. The operating parameters were set at desired values (see Table 2) after which time was allowed for stabilisation of measured parameters to be achieved. Each test took at least half an hour, including the time required for measurements of temperature, pressure and gas concentration at different points of the facility, as indicated in Fig. 1.

3. Results

CO emissions at the exit of the riser as a function of the fluidization velocity U in the riser for both bio-fuels are shown in Fig. 3 with indication of error bars. The experimental points were obtained at fixed value of the excess air factor (e = 1.27). The relatively high values of CO emissions were associated with the low temperature of combustion which was in the range 710–730 °C. Segregation phenomena in the bottom half of the riser also contributed to high CO emissions. The CO concentration increases proportionally with U as a consequence of the decreasing residence time in the riser vessel. Comparing the two fuels, bio-diesel behaves better than sunflower oil in terms of CO emissions; this can be ascribed to the better atomisation behaviour of bio-diesel that favours the formation of smaller and more easily burnable droplets emerging from the injector.

Table 2
Operating conditions of experiments

Bed material	Quartzite
Particle size (mm)	0.15–0.40
Bed inventory (kg)	20
Combustor temperature (°C)	690–770
External bed temperature (°C)	550–650
Excess air factor (–)	1.2–1.32
Fluidization velocity in the riser (m s^{-1})	2.2–2.6
Fluidization velocity in the fluidized bed (m s^{-1})	0.08–0.013
Air dispersion velocity (m s^{-1})	50–100

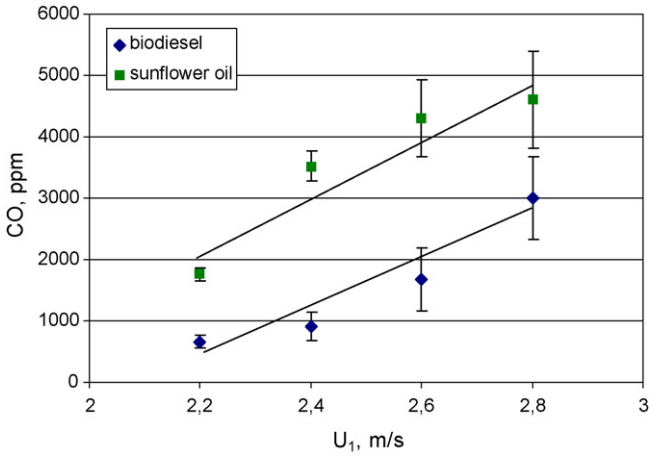

Fig. 3. CO concentration at the riser exit versus the fluidization velocity at fixed excess air factor and bed temperature (e = 1.27, T_{bed} = 983/1003 K).

Fig. 4 shows the temperature increase ΔT_{max} in the combustion zone versus U for the same tests from which Fig. 3 was compiled. ΔT_{max} is calculated as the maximum difference between the three average temperatures (T_1, T_2, T_3) measured along the riser. The

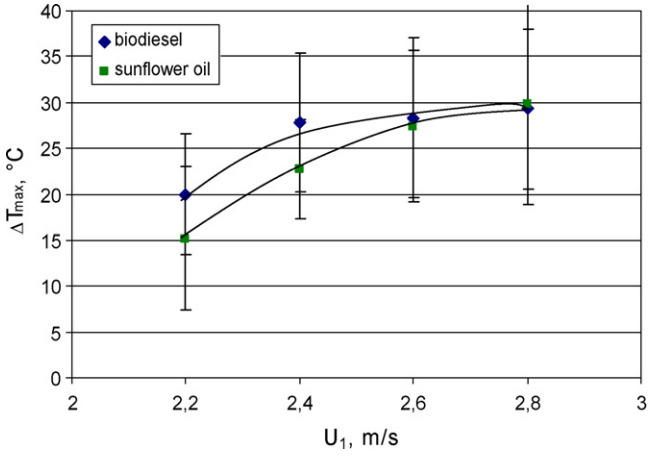

Fig. 4. Temperature increase in the riser versus fluidization velocity at fixed excess air factor and bed temperature (e = 1.27, T_{bed} = 983–1003 K).

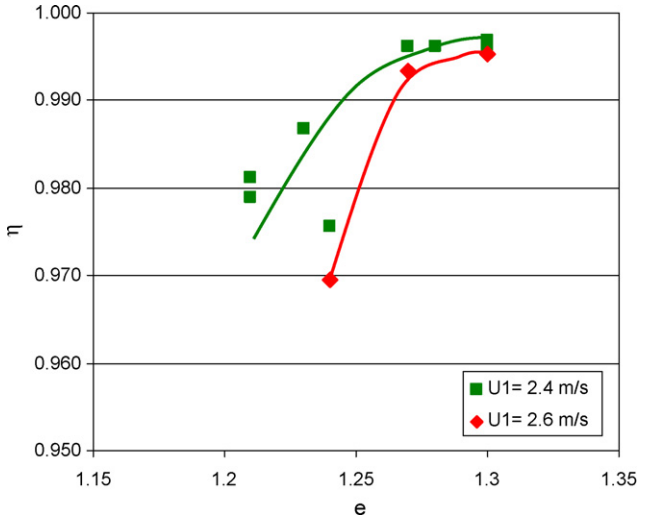

Fig. 5. Combustion efficiency in the riser versus the excess air factor for sunflower oil tests (T_{bed} = 1033 K).

error bars are also reported in the figure indicating large fluctuations of the signals. Both fuels exhibit a moderate ΔT_{max} (i.e. less than 30 °C) but it increases appreciably with increasing U. Thanks to the bed entrainment and sand circulation, the effective heat transfer between gas and bed particles keeps the temperature increase to relatively low values, even in the diluted upper zone of the riser. Increasing U leads to a linear increase of the thermal power as well as to enhance the bed circulation rate. Consequently, there is a weak influence of the fluidization velocity on ΔT_{max} which asymptotically increases with U.

Fig. 5 shows the dependence of the combustion efficiency, $\eta = 1 - Y_{CO}/(Y_{CO_2} + Y_{CO})$, on the excess air factor, e, in the combustion zone. The figure shows data for sunflower oil tests performed at temperature T_1 in the range 730–760 °C and a fluidization velocity U = 2.4 m/s. The combustion efficiency is always above 0.97 and increases at higher excess air, approaching the upper limit value of 0.998.

The emission of nitrogen oxides (NO_x) was in the range 60–90 ppm for both fuels. In order to explain this good figure, it is important to highlight the fact that the relatively low temperature in the combustor chamber inhibits the formation of thermal NO_x. Furthermore, CO emissions higher than approximately 1000 ppm generally reduce NO_x formation through the contribution of the reaction NO + CO = CO_2 + 1/2 N_2. In contrast, low N content in liquid fuels favours high conversion of nitrogen to NO_x during FB combustion [14]: at very low N-content the conversion to NO_x is tending to 100%. Also, good dispersion of liquid fuel in FB results in lower CO emissions and slightly higher NO_x emissions [15]. The higher sand concentration in bubbling FBs is reported to cause lower CO emissions and practically constant NO_x emissions [15]. In conclusion, in the case of liquid fuels with nitrogen content less than 250 ppm, the NO_x emissions during FB combustion are low and in general below the limits set by environmental emissions legislation.

Fig. 6 shows the pressure diagram for P_1 and P_4 transducers, located at the bottom and at the exit of the internal vessel, respectively. The measurements were taken in a short time sequence during a sunflower oil test carried out at temperature T_1 between 500 and 550 °C. The dynamic change of the pressure is clearly depicted in the three panels. Together with fluid-dynamic fluctuations (P_1) there are a few pressure peaks that are clearly shown in the diagram for P_4. The pressure peaks originate from the bursting of air-fuel bubbles in the bed, or immediately above it. These

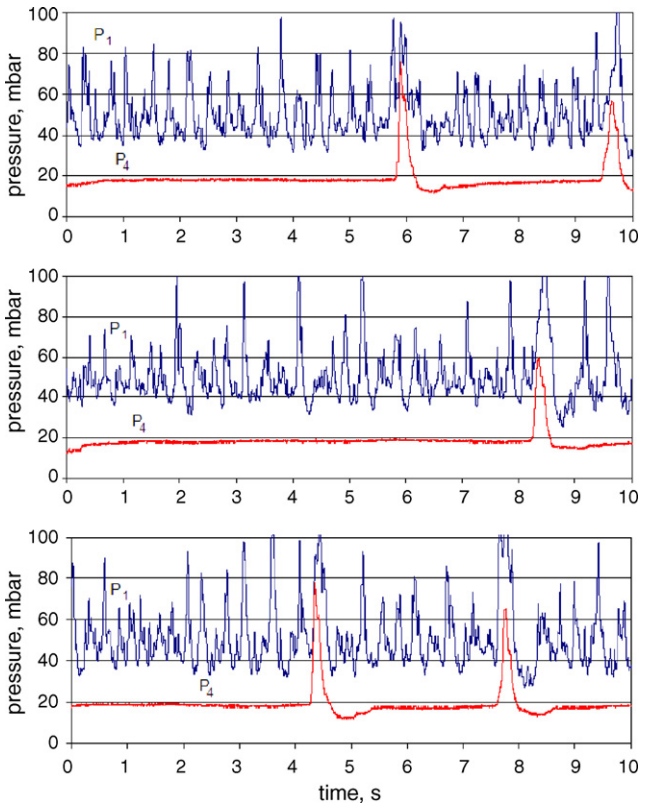

Fig. 6. Three pressure diagrams acquired in short sequence during a sunflower oil experiment (e = 1.25, T_{bed} = 773–823 K).

phenomena already have been observed for bubbling bed combustion of diesel fuel [10] and referred to as micro-explosions. It is worth noting that the fluid-dynamic fluctuations are not strong enough to completely override the pressure peaks induced by micro-explosion, as shown in the diagram for P_1.

Fig. 7 shows the pressure data taken at the exit of the riser (P_4) for a sunflower oil test carried out under transitory conditions. The temperature has been increased from 500 °C up to 770 °C at constant excess air factor e = 1.21. On the left side of the data plot several pressure peaks are shown, indicating the occurrence of uncontrolled combustion phenomena (micro-explosions). Analysis of the pressure diagram reveals that under the chosen conditions of test the frequency of micro-explosions is relatively low. For the test of Fig. 7, an average period of around 10 s between pressure peaks has been calculated by counting the number of peaks in the interval 0–700 s (Fig. 7a), corresponding to the temperature range 500–600 °C. The average time between two successive micro-explosions turns out considerably longer than for experiments carried out with bio-fuels in a bubbling bed at similar values of temperature and excess air [8,10].

4. Modelling

An existing model for liquid fuel combustion in a fluidized bed [16] has been adapted and improved in order to explain the experimental trends of carbon monoxide emissions, combustion efficiency, and temperature increase along the reactor axis. The main assumption is that the combustion zone (riser) consists of a bottom slugging bed and a freeboard [17], where a steady upwards flow of entrained solids is established. In the lower region of the bed, the fuel is injected via an air assisted injector forming fuel-rich bubbles, referred to as endogenous bubbles. The fuel evaporation

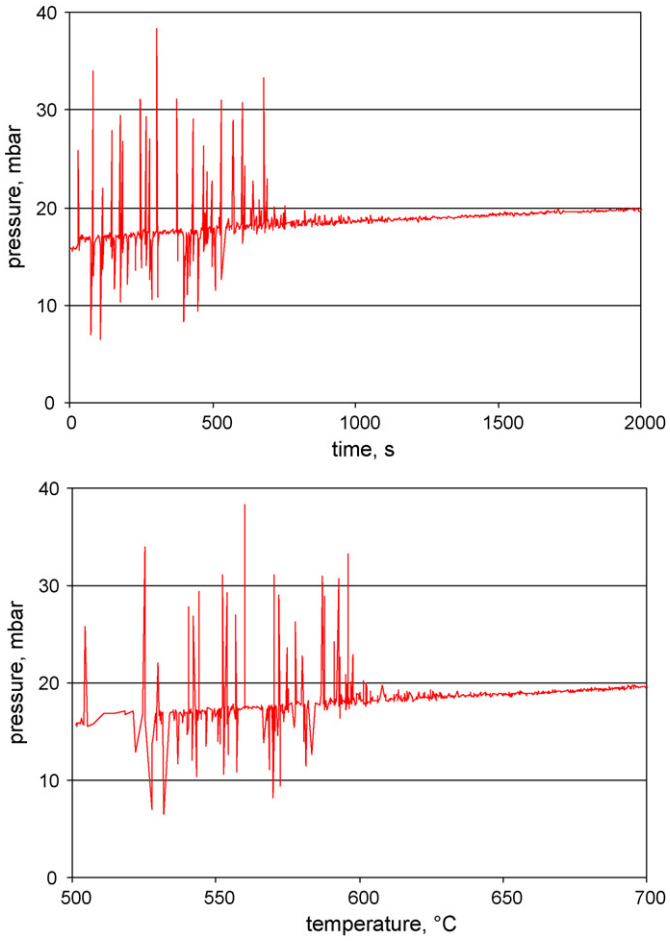

Fig. 7. Pressure diagrams at the riser exit (P_4) during a sunflower oil test at fixed excess air factor and increasing temperature ($e = 1.25$).

is very fast according to Okasha and Miccio [18]. The relationship $\Phi_{ed} = 6Q_0/(\Pi D_{b,0}^3)$ exists between the bubble frequency, the initial bubble size $D_{b,0}$ and the volumetric flow rate, Q_0, of the fuel/air jet.

The fluidized bed has uniform and constant temperature and behaves in slugging mode, so the air required for minimum fluidization can be neglected with respect to the air flow in slugs ($U_{mf} \ll U$). The slug size is assumed equal to the fraction 7/10 of the tube diameter D_t. Under the hypothesis of a spherical slug shape, the relation $\Phi_{sl} = 3UD_t^2/(2D_{sl}^2)$ exists between the slug frequency Φ_{sl} and the fluidization velocity, U. Discrete coalescence events between endogenous bubbles and slugs may occur, improving the mixing between fuel and air.

A simplified kinetic scheme based on eight chemical reactions (R1–R8) is adopted for the pyrolysis and oxidation of the vaporised fuel upon injection into the bed. According to experimental studies of Herbinet et al. [19], the pyrolysis of dodecane gives CH_4, C_2H_4, C_3H_6, and H_2 as main products (reactions R1–R3). Methane is partly oxidised by lumped reaction R4, whereas C_2H_4 and C_3H_6 are converted to hydrogen and carbon monoxide in lumped steps R4–R6 [20]. Reactions R7 and R8 account for the oxidation of H_2 and CO. The kinetic parameters are reported in Table 3.. For reactions R1–R3 these parameters have been calculated by best fitting of experimental data of conversion degree [19], whereas for reactions R4–R8 the kinetic parameters have been taken from the available literature [20–22].

Table 3
Kinetic data for chemical reactions

Reaction	k ($L^{\nu-1}\,mol^{1-\nu}\,s^{-1}$)	E ($J\,mol^{-1}$)	ν
R1	2.0×10^{10}	200,000	1
R2	2.0×10^{10}	200,000	1
R3	1.4×10^{10}	200,000	1
R4	1.6×10^{13}	200,000	1.5
R5	5.0×10^{14}	200,000	1.75
R6	5.0×10^{14}	200,000	1.75
R7	1.8×10^{13}	146,000	1.5
R8 forward	4.0×10^{14}	167,200	1.75

(R1) $C_{12}H_{26} \rightarrow CH_4 + 5.5C_2H_4$ $+555\,kJ\,mol^{-1}$

(R2) $C_{12}H_{26} \rightarrow 6C_2H_4 + H_2$ $+655\,kJ\,mol^{-1}$

(R3) $C_{12}H_{26} \rightarrow 4C_3H_6 + H_2$ $+423\,kJ\,mol^{-1}$

(R4) $CH_4 + 1.5O_2 \rightarrow CO + 2H_2O$ $-519\,kJ\,mol^{-1}$

(R5) $C_2H_4 + O_2 \rightarrow 2CO + 2H_2$ $-271\,kJ\,mol^{-1}$

(R6) $C_3H_6 + 1.5O_2 \rightarrow 3CO + 3H_2$ $-348\,kJ\,mol^{-1}$

(R7) $H_2 + 0.5O_2 \rightarrow H_2O$ $-242\,kJ\,mol^{-1}$

(R8) $CO + 0.5O_2 \leftrightarrow CO_2$ $-283\,kJ\,mol^{-1}$

The homogeneous reactions take place in both endogenous bubbles and freeboard at rates r_i depending on the composition of the gaseous system and temperature via the Arrhenius formula (Eq. (1)).

$$r_i = k_i \exp\left(-E_i \frac{R}{T}\right) \Pi_j C_j^{\nu} \tag{1}$$

Although (R8) is reversible, the contribution of the back reaction is negligible at relatively low temperature ($T < 1800$ K), the thermodynamic equilibrium favouring the forward one.

The conservation equation for a generic species i (i.e. O_2, N_2, CO_2, H_2O, CO, CH_4, H_2, C_2H_4, C_3H_6) in the endogenous bubble reads:

$$\frac{d}{dt} n_{b,i} = \frac{\pi}{6} D_b^3 \sum r_i \beta_i + \Omega_i \tag{2}$$

where Ω_i represents the molar transfer rate of species i from an air slug upon a coalescence event occurring at arbitrary time. It is worth noting that Ω_i turns out null for each species, except for O_2 and N_2.

The energy equation for the endogenous bubble is given by Eq. (3):

$$n_b c_g \frac{d}{dt} T_b = \frac{\pi}{6} D_b^3 \{h_{be}(T_{bed} - T_b) + \sum_j r_j \zeta_j\} + \Omega_i c_g (T_{bed} - T_b) \tag{3}$$

where ζ_j is the enthalpy of the generic chemical reaction j.

The coefficient h_{be} of thermal exchange between the bubble and the bed emulsion [23] is calculated via Eq. (4).

$$h_{be} = \left\{ 4.5 \left(\frac{U_{mf} C c_g}{D_b}\right) + 5.85 \left(\frac{\sqrt{k_t C c_g} g^{0.25}}{D_b^{1.25}}\right) + \frac{0.25 c_g C U_b A_p}{1000} \left[1 - \exp\left(-\frac{6\beta_p \sqrt{1.14 D_b g^{-1}}}{c_g C D_p}\right)\right] \right\} \frac{D_b}{6} \tag{4}$$

where β_p is estimated by the Ranz and Marshall correlation [24].

Eqs. (5) and (6) provide the bubble and slug velocities, respectively [23,25].

$$U_b = 1.6[(U - U_{mf}) + 1.13\sqrt{D_b}]D_t^{1.35} + 0.711\sqrt{gD_b}\exp\left(-1.49\frac{D_b}{D_t}\right) \quad (5)$$

$$U_{sl} = (U - U_{mf}) + 0.35\sqrt{gD_t} \quad (6)$$

The coalescence between an endogenous rising bubble and a slug occurs once inside the bed and takes a time θ proportional to the bubble size divided by the difference between the rising velocities (Eq. (7)). The consequent change of the bubble volume and enthalpy is computed following Miccio and Ferrante [16].

$$\theta = \frac{D_b}{|U_{sl} - U_b|} \quad (7)$$

The freeboard is modelled as a non-isothermal plug flow reactor, where the endogenous bubbles are continuously fed. Furthermore, the current originating from the air slugs is gradually and uniformly added to the fuel-rich plug flow, likewise a not-premixed burner. Therefore, a diffusion flame establishes downstream the bed, whose length $\lambda = 0.108d\,Re$ is estimated as function of the Reynolds number Re following Sunderland et al. [26]. The orifice size d is computed as the equivalent diameter of the tube section multiplied by the ratio between the volumetric flow rate of bubbles and total flow rate. Considering the pulsing behaviour of the bubbles and slugs that exerts a detrimental effect on the flame length, the coefficient 0.108 has also been increased by a factor 1.5.

The conservation equation for a generic species i (i.e. O_2, N_2, CO_2, H_2O, CO, CH_4, C_2H_4, C_3H_6, H_2) in the freeboard reads:

$$\frac{P}{RT}U\frac{dY_i}{dz} = \sum_j r_j\beta_i + \Psi_i \quad (8)$$

where Ψ_i is the flux transferred from the slug current to the reactive flow. It is roughly estimated by uniformly distributing the whole slug current along the whole flame length λ.

The energy equation (Eq. (9)) allows the computation of the temperature profile in the freeboard, where the difference between the combustion energy and that transferred to the wall heats up both gas stream and entrained solid stream.

$$\left(\frac{P}{RT}Uc_g + W_s c_s\right)\frac{dT}{dz} = \sum_j r_j\zeta_j - \frac{4}{D_t}h_w(T - T_{bed}) \quad (9)$$

The mass flow rate of solids, W_s, is a function of the fluidization velocity in the riser U, the terminal velocity U_t and the total bed inventory W_{bed}, as reported by Miccio et al. [27].

$$W_s = K\sqrt{W_{bed}}(U - U_t) \quad (10)$$

The initial conditions ($z = 0$) for the freeboard are $Y_i UA = Y_{b,i}V_b\Phi_b$ and $T_{fr,0} = T_{bed}$. The number of coalescence events has been assumed to be equal to one, meaning that an endogenous bubble coalesces with a slug once during its life. This event occurs at half of the bed height. It is worth noting that after coalescence the bubble volume becomes larger than the slug volume. All other variables and parameters have been set at values close to those of the experiments (Table 2).

The differential equations have been solved by numerical integration with Euler method adopting a self-variable time step. The outputs for the bed zone are passed in sequence as inputs for resolving the freeboard zone. The model computes the axial profiles of relevant variables, including gas concentrations, molar fluxes and temperature. For the base case computation the following values are assumed: $H = 0.3$ m, $U_0 = 50\ m\,s^{-1}$, $e = 1.25$, $U = 2.5\ m\,s^{-1}$, $T_{bed} = 985$ K, $\Phi = 12$ Hz, $K = 1563\ kg^{0.5}\,m^{-1}$.

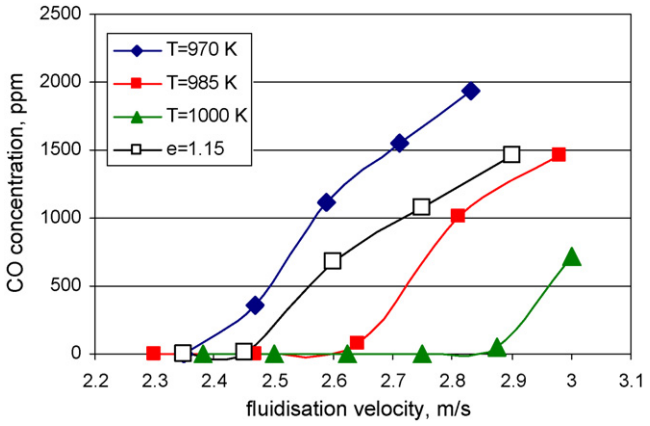

Fig. 8. CO concentration versus the fluidization velocity as predicted by the model, ($H = 0.3$ m, $U_0 = 50\ m\,s^{-1}$, $K = 1564\ kg^{0.5}\,m^{-1}$, $\Phi = 12$ Hz).

5. Discussion

Figs. 8 and 9 report selected outputs of the model, namely the CO concentration at the riser exit Y_{CO} and the temperature increase ΔT versus the fluidization velocity, for different values of the bed temperature T_{bed} and excess air factor. The values and the trend of the CO concentration are in satisfactory agreement with the experimental results of Fig. 3. Nevertheless, a different behaviour is predicted by the model with a sharp transition from a low emission to a high emission regime at increasing fluidization velocity. The threshold effect is explained by considering that the flame length in the freeboard also increases with U, so the narrow zone where CO is converted to CO_2 approaches or exceeds the combustor exit. Lower CO emissions at increasing the bed temperature as well as the excess air ratio are congruently predicted by the model.

In contrast with the experimental results of Fig. 4, the model predicts a higher ΔT and an inverted trend at increasing U, as depicted in Fig. 9. This model failure, more marked at lower fluidization velocity, must be attributed to underestimated mixing between fuel and air in the bed zone as a consequence of the simplified bed fluid-dynamic. The influence of the excess air factor for both CO concentration and temperature increase is straightforward: the

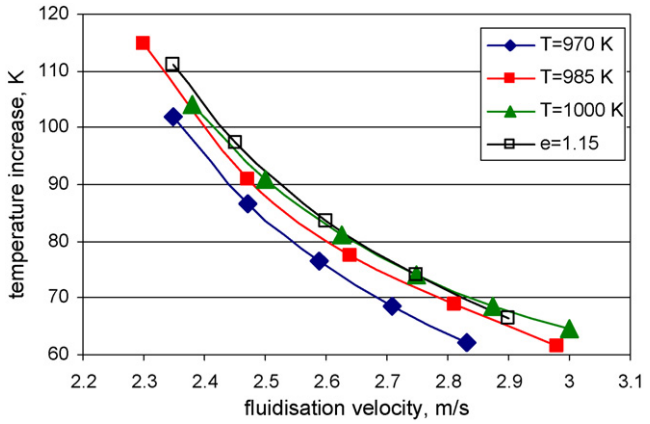

Fig. 9. Temperature increase versus the fluidization velocity as predicted by the model, ($H = 0.3$ m, $U_0 = 50\ m\,s^{-1}$, $K = 1564\ kg^{0.5}\,m^{-1}$, $\Phi = 12$ Hz).

higher e, the lower are Y_{CO} and ΔT, because of the increased dilution in air and availability of oxygen. An appreciable effect on the temperature increase is also exerted by T_{bed} (Fig. 9) because at higher bed temperature the mixing in the bed via coalescence mechanism is depressed by the lower air density. On the whole, the calculations demonstrate that the mixing between fuel and air in the bed has a prominent influence on the combustion performance and CO emissions.

It must be remarked that all other parameters have been kept constant during model computations. In particular the bubble frequency at the injector has been set at 12 Hz, corresponding to bubble size in the range 30–40 mm. Therefore, a sensitivity analysis following the standard procedure by Rudd and Watson [28] has been carried out to check the influence of relevant input variables/parameters on the model performance, assuming as output the temperature increase ΔT. The sensitivity σ is given by the following expression:

$$\sigma = \frac{[(O^- - O^+)/O_b]}{[(I^- - I^+)/I_b]}$$

The result is reported hereinafter as the sequence by which parameters/variables exert their influence, listed in the order of their relative importance. The sensitivity index is also reported inside the brackets.

(1) U (2.69)
(2) T_{bed} (2.58)
(3) K (0.99)
(4) e (−0.61)
(5) Φ = 0.16
(6) U_0 (−0.02)

6. Conclusions

Two liquid bio-fuels have been burnt in an internal circulating fluidized bed under conditions suitable for co-gasification of biomass/waste materials. Fuel feeding by means of an air-assisted injector, coaxial with the combustion riser, has been smooth and reliable. High combustion efficiency and limited temperature increase along the riser have been attained under different operating conditions. However, improvements in CO abatement are needed. Nitrogen oxides have been under 100 ppm for all tests performed. A high bed circulation rate is beneficial for keeping the temperature increase along the riser at low values. No large differences have been noted in the operation with the two bio-fuels.

Micro-explosions have been experienced in the fluidized bed in the temperature range 500–600 °C as a consequence of the bursting of fuel-air bubbles. However, the frequency at which they occur seems significantly lower that that measured under bubbling bed conditions. This is a clear demonstration that the instability phenomena of micro-explosions is minimised in ICFB.

A theoretical approach has been proposed for the interpretation of the experimental findings leading to the development of a model based on coalescence at the bottom of the bed and multiple-step kinetics. The agreement between experimental and model results is rather good, although the temperature increase in the freeboard is overestimated. However, the model demonstrates, that the mechanism of fuel-air mixing has a crucial role in achieving good combustion performances.

The sensitivity analysis of model inputs has shown that the fluidization velocity and the bed temperature have the greatest importance. Nevertheless, some parameters, namely the bubble frequency and the bed circulation rate, deserves a careful evaluation, since their are not easily measurable with direct techniques.

Although the experimental campaign has been limited and scale-up should also be taken into account, the research strengthens the idea to utilize the ICFB process for co-gasification of biomass supported by liquid bio-fuels or for incineration of liquid wastes, such as contaminated or used oils.

References

[1] L. Ferrante, Studies on Mechanism of Liquid Fuel Combustion in Bubbling Fluidized Bed, PhD Thesis in Chemical Engineering, Università di Salerno. (2007).
[2] Y. Eniakin, M. Zaizeva, M. Maidanik, E. Bojevolnova, N. Maslennikova, A. Pojogina, V. Terzieva, Investigation of residual oil combustion in the fluidized bed of an inert granular material, Teploenergenika 12 (1980) 33–36.
[3] D. Barker, B. Beacham, Development and commercial application of liquid-fuelled fluidised combustion, Proceedings of the Institute of Fuel International Conference, London (UK), 1980, I-A3.
[4] R. Legros, C.J. Lim, C.M.H. Brereton, J.R. Grace, Circulating fluidized bed combustion of pitches derived from heavy oil upgrading, Fuel 70 (1991) 1465–1471.
[5] B. North, C. Eleftheriades, A. Engelbrecht, Incineration of a biomass sludge in a bubbling FBC, in: 15th International Conference of Fluidized Bed Combustion, Asme, Savannah, USA, 1999, pp. 153–163.
[6] J. Zhang, D.Y. Lu, E.J. Anthony, The fluidized bed combustion of heavy liquid fuels, in: 16th International Conference of Fluidized Bed Combustion, Asme, Reno Nevada, USA, 2001, pp. 1041–1055.
[7] F.M. Okasha, S.H. El-Emam, H.K. Mostafa, The fluidized bed combustion of a heavy liquid fuel, Exp. Thermal Fluid Sci. 27 (2003) 473–480.
[8] L. Ferrante, M. Miccio, R. Solimene, F. Miccio, An investigation on low-temperature fluidized combustion of liquid fuels, 18th FBC Conf., ASME (2005) 433–441.
[9] M. Fiorentino, A. Marzocchella, P. Salatino, Segregation of fuel particles and volatile matter during devolatilization in a fluidized bed reactor. II. Experimental, Chem. Eng. Sci. 52 (1997) 1909–1922.
[10] F. Miccio, M. Miccio, G. Olivieri, A. Silvestre, On the mechanism of bubbling fluidized bed combustion of gasoil, Ind. Eng. Chem. Res. 42 (2003) 3973–3981.
[11] P. McKendry, Energy production from biomass: gasification technologies, Bioresour. Technol. 83 (2002) 55–63.
[12] H. Hofbauer, G. Veronik, T. Fleck, R. Rauch, H. Mackinger, E. Fercher, The FICFB Gasification Process Proceedings of Developments in Thermochemical Biomass Conversion, 2, Banff, 1016, 1997.
[13] H. Hofbauer, Scale Up of Fluidized Bed Gasifiers from Laboratory Scale to Commercial Plants: Steam Gasification of Solid Biomass in a Dual Fluidized Bed System, Proceedings of 19th FBC Conference, Vienna, CD, 2006.
[14] K. Svoboda, M. Hartman, Formation of NO_x in fluidized bed combustion of model mixtures of liquid organic compounds containing nitrogen, Fuel 10 (1991) 865–871.
[15] F.M. Okasha, S.H. El-Emam, H.K. Mostafa, The fluidized bed combustion of a heavy liquid fuel, Exp. Therm. Fluid Sci. 27 (2003) 473–480.
[16] F. Miccio, L. Ferrante, Fluidized bed combustion of a diesel fuel: a modeling interpretation for micro-explosions, Proc. Combust. Inst. 31 (2007) 2821–2828.
[17] A. Svensson, F. Johnsson, B. Leckner, Bottom bed regimes in a circulating fluidized bed boiler, J. Multiphase Flow 22 (1996) 1187–1204.
[18] F.M. Okasha, M. Miccio, Modeling of wet jet in fluidized bed, Chem. Eng. Sci. 61 (2006) 3079–3090.
[19] O. Herbinet, P.M. Marquaire, F. Battin-Leclerc, R. Fournet, Thermal decomposition of *n*-dodecane: experiments and kinetic modeling, J. Anal. Appl. Pyrolysis 78 (2007) 419–429.
[20] C.K. Westbrook, F.L. Dryer, Chemical kinetic modelling of hydrocarbons combustion, Prog. Energy Combust. Sci. 10 (1984) 1–57.
[21] C. Appel, J. Mantzaras, R. Schaeren, R. Bombach, A. Inaunen, Catalytic combustion of hydrogen-air mixtures over platinum: validation of heterogeneous chemical reaction schemes, Clean Air 5 (2004) 21–44.
[22] F.L. Dryer, I. Glassman, High-temperature oxidation of CO and CH_4, Proc. Combust. Inst. 14 (1973) 987–1001.
[23] D. Kunii, O. Levenspiel, Fluidization Engineering, 61, Butterworth-Heinemann, Boston, 1991.
[24] W.E. Ranz, W.R. Marshall, Evaporation from drops, Chem. Eng. Prog. 48 (1952) 141–146.
[25] C.R. Müller, J.F. Davidson, J.S. Dennis, P.S. Fennell, L.F. Gladden, A.N. Hayhurst, M.D. Mantle, A.C. Rees, A.J. Sederman, Rise velocities of bubbles and slugs in gas-fluidised beds: ultra-fast magnetic resonance imaging, Chem. Eng. Sci. 62 (2007) 82–93.
[26] P.B. Sunderland, B.J. Mendelson, Z.-G. Yuan, D.L. Urban, Shapes of buoyant and nonbuoyant laminar jet diffusion flames, Combust. Flame 116 (1999) 376–386.
[27] F. Miccio, K. Svoboda, J.P. Schosger, D. Baxter, Biomass gasification in internal circulating fluidized beds: a thermodynamic predictive tool, Korean J. Chem. Eng. (2008), in press.
[28] D.F. Rudd, C.C. Watson, Strategy of Process Engineering, Wiley, New York, 1968.